

Application of the H/V Spectral Ratios for Earthquake Ground Motions and Microtremors at K-NET sites in Tohoku Region, Japan to Delineate Soil Nonlinearity



15 WCEE
LISBOA 2012

F. Nagashima, H. Kawase & S. Matsushima

DPRI, Kyoto University, Japan

F. J. Sánchez-Sesma

Instituto de Ingeniería, Universidad Nacional Autónoma de México Mexico

T. Hayakawa, T. Satoh & M. Oshima

Institute of Technology, Shimizu Corporation, Japan

SUMMARY

We have proposed an optimal way to use horizontal-to-vertical (H/V) spectral ratios for underground structure exploration, which is based on diffuse field concepts (Sanchez-Sesma et al., 2011; Kawase et al., 2011). This approach is applicable to earthquake and microtremor ground motions. We show here analysis on the observed data around K-NET station in Japan where very large peak ground acceleration was observed. We compare H/V spectral ratios of the strong motions during the Off the Pacific Coast of Tohoku Earthquake of March 11, 2011 with those averaged over several weak motions to see soil nonlinearity effects on the H/V spectral ratios. After we determine detailed velocity structures based on the H/V spectral ratios of the seismic motions, we estimate deconvolved bedrock motions during main shock considering nonlinearity and then simulate strong motions around the K-NET station.

Keywords: Tohoku earthquake, Nonlinear soil amplification, H/V Spectral Ratio

1. INTRODUCTION

During the 2011 Off the Pacific Coast of Tohoku Earthquake that occurred on March 11, 2011, the maximum acceleration of the NS component reached $2,700 \text{ cm/s}^2$ and JMA seismic intensity 7 was recorded at K-NET Tsukidate (MYG004) station, Miyagi, Japan, of the K-NET strong motion network (for the network description see Kinoshita, 1998). However, damages near the observation site were quite limited. The authors, therefore, observed aftershocks around MYG004 in order to identify factors for generating high acceleration and investigate the relationship between high acceleration and damages in the vicinity. Also, prior to the aftershock observation, we measured microtremors to focus on the effect of cliff topography near MYG004. The H/V spectral ratios (HVRs) of these data were compared to identify the ground motion characteristics of the area, and the HVRs of ground motion records were used to identify the soil structure around MYG004. We estimated the bedrock seismic motion of the main shock using deconvolution analysis, and simulated the strong motions at the temporary observation sites.

2. TEMPORARY AFTERSHOCK OBSERVATION AT TSUKIDATE

On April 29 and 30, 2011, four survey sites were deployed around MYG004. One site was set at the center and other three sites were set on the circumference of a circle with a diameter of approximately 400 m around MYG004. Fig. 2.1 shows the locations of MYG004 and temporary aftershock observation sites (TKDZ01~TKDZ04). At these sites, data have been continuously recorded using SMAR-6A3P (Mitutoyo Corporation), in which the data logger was replaced by LS8800 (Hakusan Corporation). These sites were set under eaves of residential properties with AC power. GPS was used for time correction and data sampling had been performed at 100 Hz.



Figure 2.1. Locations of the observation sites in Tsukidate, Kurihara City.

3. INFLUENCE OF THE CLIFF TOPOGRAPHY

3.1. Microtremor observation

Before deploying the temporary aftershock observation sites, in order to determine the effects of the cliff topography near MYG004, microtremor array observation was performed at five sites: two sites were set on top of the cliff and three sites were set at the base of the cliff. Fig. 3.1 shows the array arrangement. M01 and M02 were set on top of the cliff with M02 located right in front of MYG004, and M01 was set approximately 10 m south of M02. M03, M04 and M05 were set at the base of the cliff with M03 located immediately beneath the cliff and M4 and M05 located 10 m and 30 m apart from M03, respectively. Microtremors were recorded for 30 minutes.

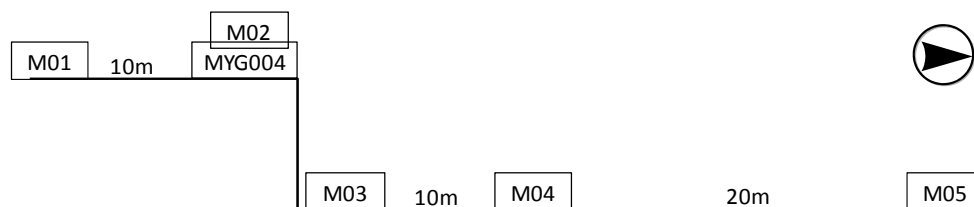


Figure 3.1. Schematic figure of microtremor array arrangement across the cliff near MYG004.

3.2. Microtremor HVRs

HVRs were computed for the NS and EW components from average Fourier spectra, separately. Figs. 3.2 and 3.3 show the HVRs for NS/UD and EW/UD respectively. While the HVRs at all the five sites were similar to each other up to 7 Hz, for frequencies higher than 7 Hz, the HVRs for the cliff-top sites (M01 & M02) were two to three times as high as the HVRs for the cliff-base sites. This is believed to be the effect of the cliff topography.

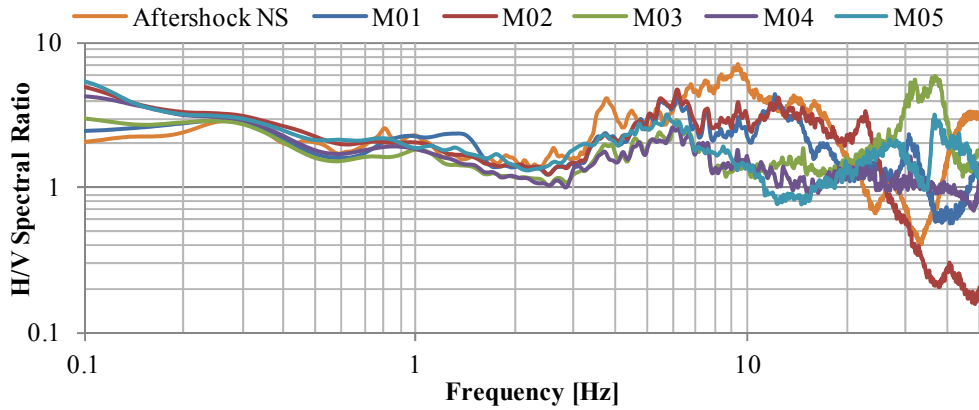


Figure 3.2. Microtremor HVRs of the linear array with aftershock HVR for MYG004 (NS/UD).

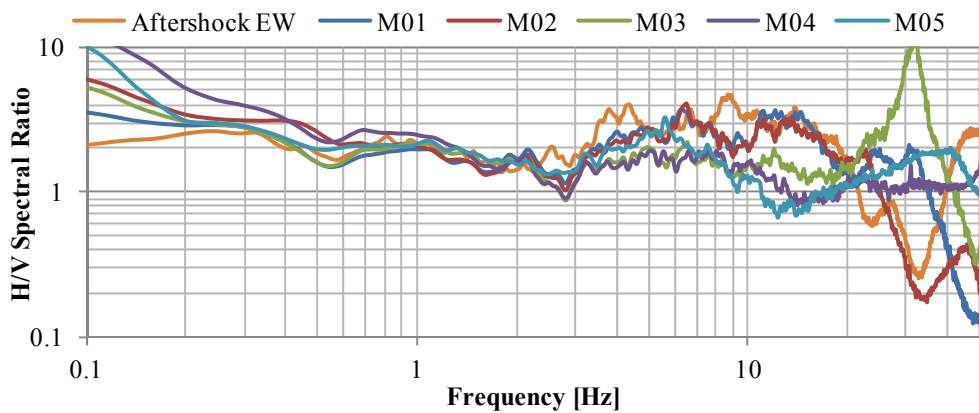


Figure 3.3. Microtremor HVRs of the linear array with aftershock HVR for MYG004 (EW/UD).

4. AFTERSHOCK DATA AT TSUKIDATE

4.1. Comparison of weak motion HVRs at temporary observation sites

From the aftershock data recorded between April 30 and September 20, 2011 at four temporary observation sites shown in Fig. 2.1., a time window of 81.92 seconds from the onset of the S wave was extracted and the average Fourier spectrum of each component was computed to determine the HVRs, that is, NS/UD and EW/UD, for the 77 earthquakes recorded at MYG004. Figs. 4.1. and 4.2. show the aftershock HVRs for NS/UD and EW/UD as well as those for MYG004, respectively. The aftershock HVRs have peaks at around 0.3 and 1.0 Hz at all five survey sites including MYG004, which seems to be the effect of the deep soil structure. On the other hand, at frequencies higher than 1.5 Hz, HVRs are significantly different among the observation sites, except for TKDZ01 and TKDZ02. The NS component at MYG004, in particular for 7~10 Hz, showed higher HVRs than those at other observation sites. This is consistent with the results discussed in the previous section, where the effects of the cliff topography were apparent at frequencies higher than 7 Hz. Note that at TKDZ04 where there were some damages occurred to buildings, a peak can be seen at around 2.5 Hz, indicating the relationship between dominant frequency and damages.

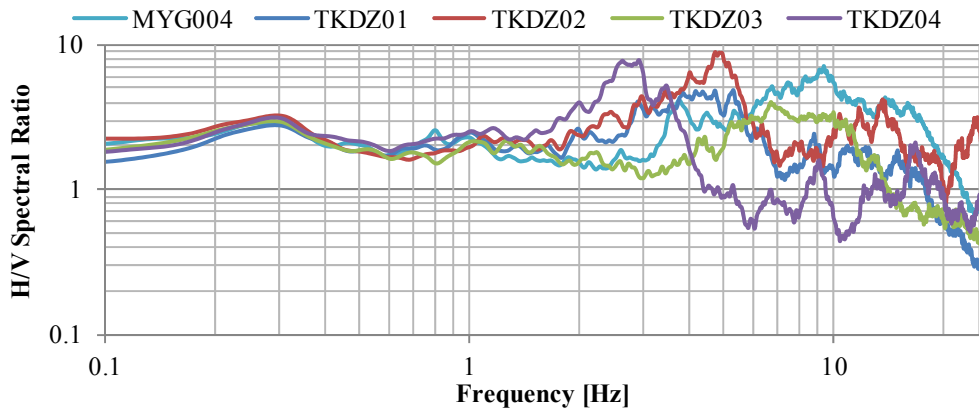


Figure 4.1. Aftershock HVRs in Tsukidate (NS/UD).

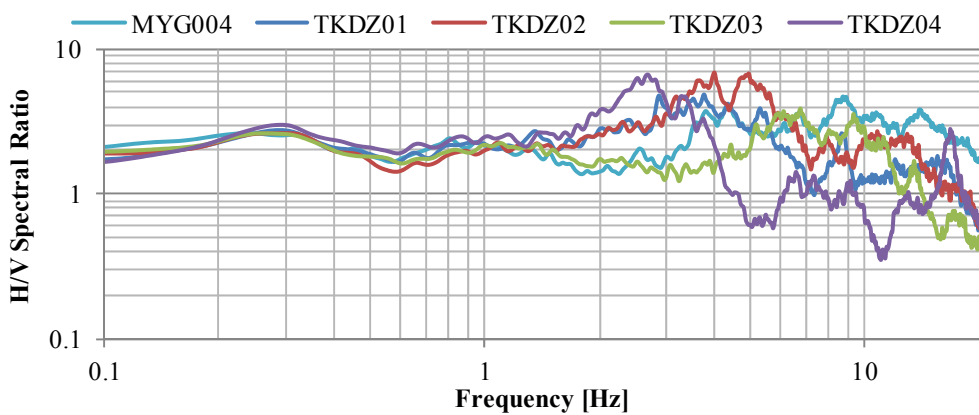


Figure 4.2. Aftershock HVRs in Tsukidate (EW/UD).

4.2. Comparison between the main shock, the April 7 largest aftershock and average of other aftershocks at MYG004

Next, we compare the strong motion HVRs of the main shock, and the largest aftershock that occurred at 23:32 on April 7 (M7.1) with average weak motion HVRs of other aftershocks. Figs. 4.3. and 4.4. compare NS/UD and EW/UD of these HVRs, respectively. With regard to the maximum acceleration (PGA), the NS and EW components for the main shock were $2,700 \text{ cm/s}^2$ and $1,268 \text{ cm/s}^2$, respectively, and those for the April 7 aftershock were $1,242 \text{ cm/s}^2$ and 886 cm/s^2 , respectively, showing large differences between the two events (1.5~2 times), but the HVRs were similar between them. Compared with the weak motion HVRs, the peaks of the strong motion HVRs were shifted to lower frequencies, indicating the effect of nonlinearity. The peak frequency was shifted from 9 Hz to 4~5Hz for strong motion HVRs in comparison to weak motions HVRs, and shear rigidity may have dropped to approximately 25 % of the linear values during the strong shaking.

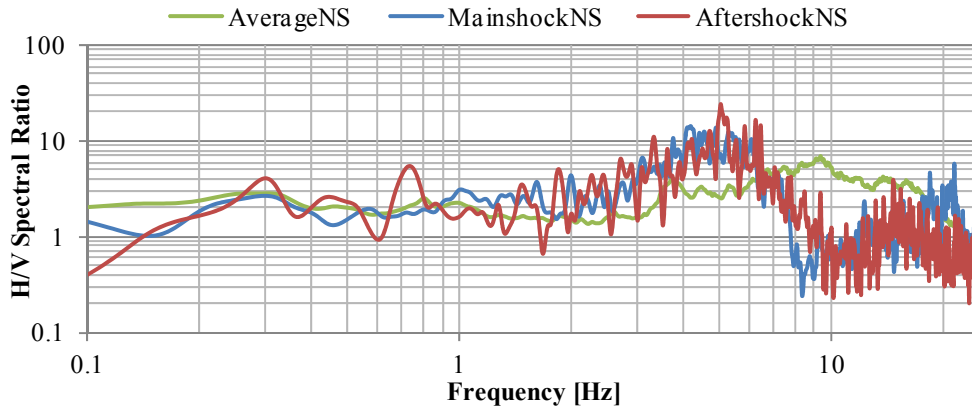


Figure 4.3. HVRs of main shock, largest aftershock and average of other aftershocks at MYG004 (NS/UD).

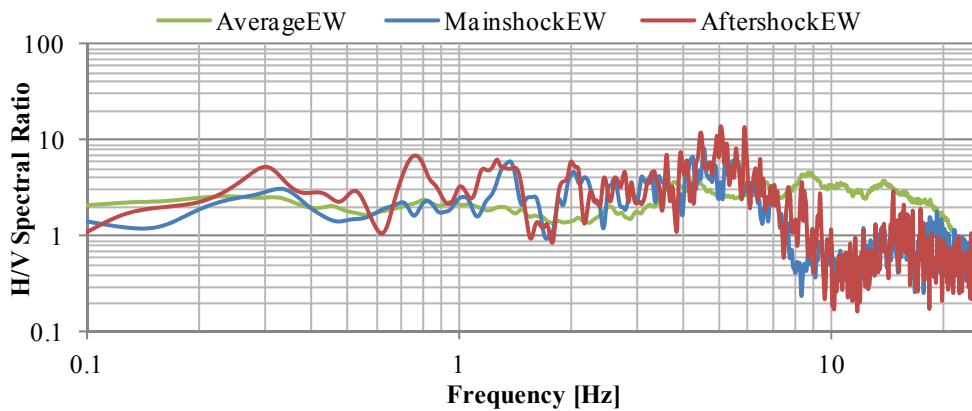


Figure 4.4. HVRs of main shock, largest aftershock and average of other aftershocks at MYG004 (EW/UD).

5. IDENTIFICATION OF THE SOIL STRUCTURE

5.1. Identification at MYG004

Identification of the soil structure immediately below MYG004 was attempted based on the HVRs of weak motion data recorded at the site. First, for the 55 waves observed between March 9 and May 17, 2011, average HVRs of the EW components, which are believed to be less influenced by the cliff topography, was used as a target to identify the soil structure at MYG004, by making the residual sum of squares smallest with theoretical HVRs. For the initial model, the data published by the National Research Institute for Earth Science and Disaster Prevention (NIED, 2011) were used for shallow soil layers and the results of previous study (Kawase and Matsuo, 2004) were used for deep soil layers. Layers 2 and 3 of the eight-layered model of Kawase and Matsuo (2004) had similar PS logging results and densities, so they are treated as one layer to make a seven-layered model (the Initial Model in Table 5.1.). The theoretical HVRs were calculated based on the concept of Kawase et al. (2011), and were identified by changing the thickness of layers 1 to 6. As a result, the velocity structure that explains the observed HVRs well was identified as shown in Fig. 5.1. The velocity structure model is shown in Table 5.1 and Fig. 5.2. Comparing the identified model with the initial model, layers near the surface got thinner and layers 5 and 6 got thicker, creating peaks at 0.3 and 1.0 Hz, and hence quite nicely reproducing the observed HVR as shown in Fig. 5.1.

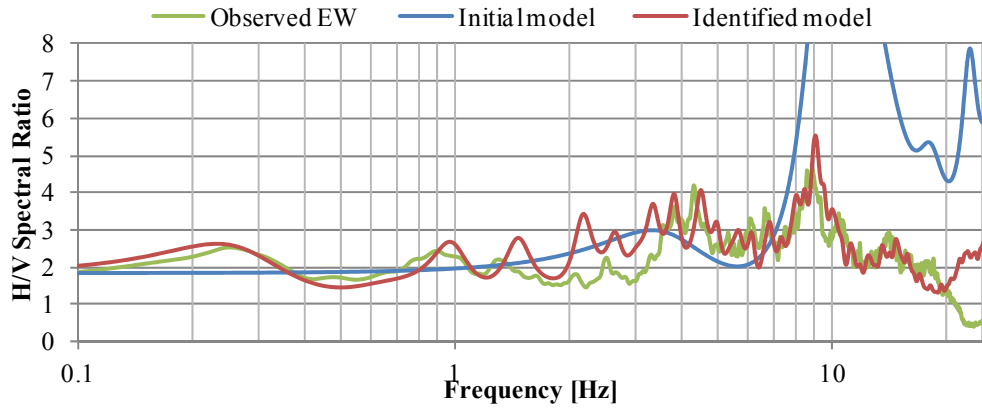


Figure 5.1. Comparison of HVRs for observed EW/UD, initial model and identified model

Table 5.1. Velocity structure of the initial and identified model

Initial Model				Identified Model	
No	Vs	Thickness	Depth	Thickness	Depth
	(m/s)	(m)	(m)	(m)	(m)
1	100	1	1	0.4	0.4
2	240	3	4	1.12	1.52
3	550	6.25	10.25	14.25	15.77
4	1364.29	20	30.25	71.4	87.17
5	2075.17	110	140.25	1624.7	1711.67
6	2874.27	50	190.25	1200	2911.67
7	3400	-	-	-	-

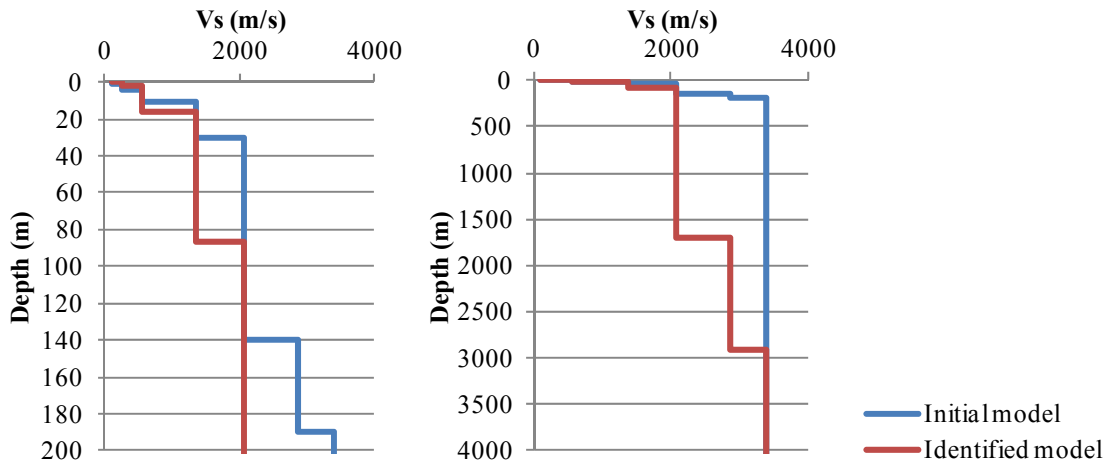


Figure 5.2. Shallow and deep part of the initial and identified velocity structures

5.2. Identification at temporary observation sites

Using the same approach adopted for MYG004, the soil structures at the temporary aftershock observation sites are identified so as to minimize the square sum of the residual difference between the observed and theoretical HVRs. For analysis of the temporary aftershock observation sites, however, a grid search is executed with the S-wave velocity as a variable in addition to the layer thickness. If there is an occurrence of an inverted layer in the S-wave velocity, such a model is discarded. The initial model was based on the model identified for MYG004 but with the following differences. The depth of the first layer was made to be very thin, at 0.4 m, and the first layer was coalesced with the

second layer under the assumption that the influence of these two different layers in the frequency range between 0.1~20 Hz used in the computation would be negligible, thus providing an initial model with a total of six layers.

The observed HVR computed at each observation site from the aftershock data was used for calculating the residual difference. There is a difference in the amplification of the peaks between NS and EW directions for observation sites TKDZ02 and TKDZ04, the mean square sum of NS and EW was used for TKDZ01 and TKDZ03, while square sums for NS and EW were used independently for TKDZ02 and TKDZ04.

The soil structures identified at the temporary aftershock observation sites are shown in Fig. 5.3. The comparison is omitted here, but we were able to obtain a model that explains the observed data very well at all observation sites. In the present analysis, the velocity structure has been identified to match each observed data. While the peaks at 0.3 Hz and 1 Hz are commonly observed across all observation sites, their power is weak, and there is insufficient resolution to determine an identical deep layer structure across all observation sites. Thus, the deep layer structure in the identified model significantly varies within short ranges. For future analyses, an identification of a model with an identical deep velocity structure would be required.

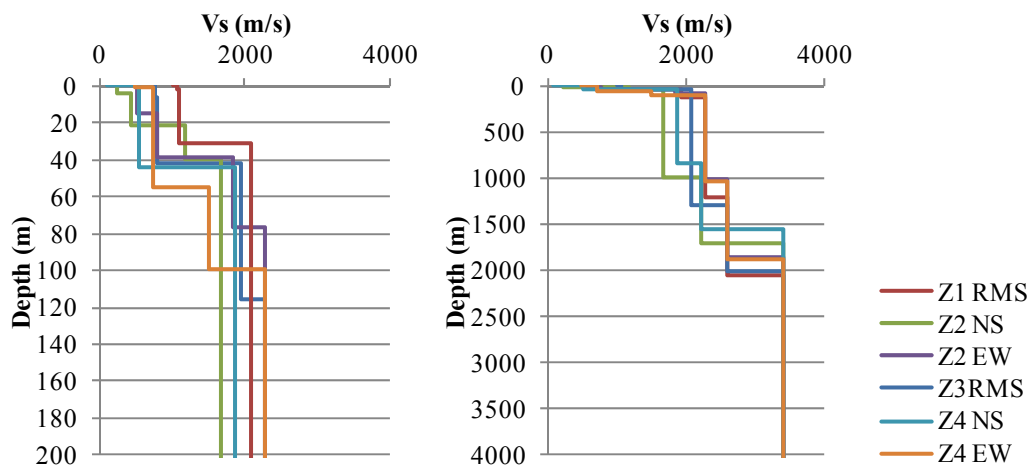


Figure 5.3. The velocity structure at temporary observation sites

6. DECONVOLUTION ANALYSIS OF INCIDENT WAVES ON BEDROCK WITH NONLINEARITY CONSIDERATIONS

6.1. Derivation of bedrock seismic motion using deconvolution analysis

Deconvolution analysis was performed to estimate the seismic bedrock wave, taking the nonlinearity of the soil structure into consideration. First, equivalent linear analysis was performed using the deconvolved wave, in which the effect of soil layers was stripped from the observed wave using the linear transmission function, as an input to obtain the equivalent linear transmission function on the ground surface. The observed wave was then deconvolved using the obtained transmission function, which was then re-injected and excited again. The above operation was repeated until a stable dynamic shear modulus, G , and damping coefficient, h , were obtained. When the changes in G and h between iterations were less than 5% for all elements, the resulting deconvolved wave was considered as the seismic wave incident to the bedrock.

6.2. Deconvolution analysis of the main shock record at K-NET Tsukidate

One-dimensional deconvolution analysis was performed on the main shock record observed at K-NET

Tsukidate to obtain the deconvolved bedrock seismic wave. The deconvolution analysis was performed by applying a filter of 0.1~20 Hz to both the NS and EW elements of the main shock data. A report has attributed the pulse-shaped acceleration at around the 100 s mark of the main shock data to rocking of the bedrock at the observation site. Thus, for the present analysis, an initial S wave part with 65-s duration was extracted between 15 s and 80 s from the start of the record.

Boring records indicate that there is soft, viscous soil up to 1.2 m in depth. This corresponds to an S-wave velocity in layers 1 and 2; thus, the nonlinear characteristics of clay (Imazu and Fukutake, 1986) were used for layers 1 and 2. Layers 3~6 are equivalent to solid rock; therefore, the nonlinear characteristics of solid rock (Fujikawa et al., 2003) were used for these layers.

Figs. 6.1 and 6.2 show the obtained deconvolved bedrock waves in blue on top of the observed surface waves. Maximum acceleration in the NS direction was 449 cm/s² and 350 cm/s² in the EW direction.

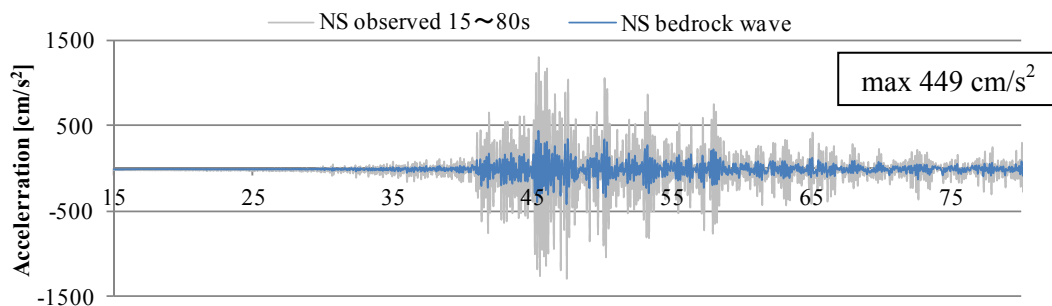


Figure 6.1. Deconvolved bedrock motion in the NS direction.

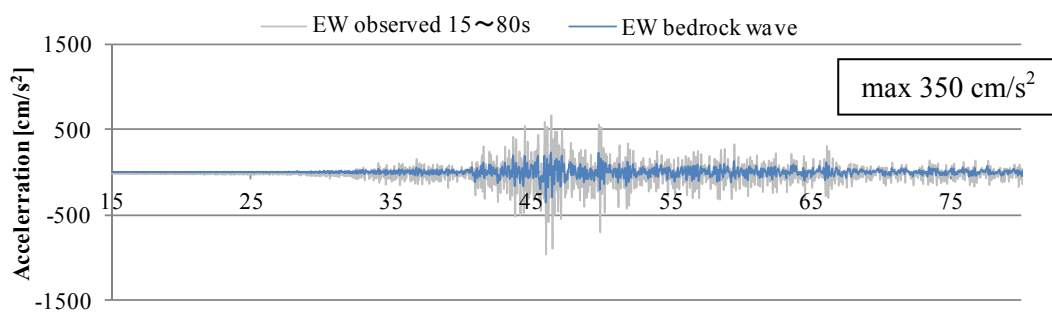


Figure 6.2. Deconvolved bedrock motion in the EW direction.

7. STRONG-MOTION SIMULATION NEAR K-NET TSUKIDATE

7.1. Simulation methodology for strong motion

A general-purpose soil response analysis code, SoilPlus (Itochu Techno Solutions), was used for computing the seismic motion at the ground surface. The identified soil structure of the temporary observation site was used to derive a one-dimensional model and the acceleration response at the ground surface was calculated using the deconvolved bedrock motion as input. In almost all sites along the identified structure at the temporary observation site, the S-wave had large velocity at the topmost layer, and the structure is thought to be a hard solid rock. Therefore, linear analysis was performed without taking the nonlinearity of the soil into consideration. The bedrock motions were injected in both NS and EW directions and analysis was performed.

7.2. Observations on the correspondence between analysis results and actual damages

Tables 7.1, 7.2, and 7.3 list the maximum acceleration, maximum velocity, maximum displacement, and JMA seismic intensity in the NS and EW direction of the observed data (top low), as well as those acquired from the strong-motion simulation (Z01~Z04). At TKDZ02, with a soil structure similar to K-NET Tsukidate, large acceleration, velocity, and displacement are observed; however, although acceleration exceeds 1 g, the velocity is in the vicinity of 50 cm/s, and displacement was only 10 cm. The seismic intensity was slightly greater than 6.0 at TKDZ02, but were lower than 6.0 at other observation sites. Although the shaking at the Tsukidate region that resulted from the initial half of the main shock had a large maximum acceleration and seismic intensity, the velocity and displacement was not so great, and it is thus believed that it did not have a large impact on building damage.

Table 7.1. Maximum acceleration, velocity, displacement, and JMA seismic intensity (NS)

	Max Acc. [cm/s ²]	Max Vel. [cm/s]	Max Dis. [cm]	Seismic intensity
Main shock 15-80s	1299.75	41.04	6.74	6.09
Bedrock wave	449.12	18.14	7.95	5.10
Z01	954.27	37.85	9.02	5.77
Z02	1473.53	50.84	11.04	6.15
Z03	571.94	33.03	9.41	5.41
Z04	559.91	32.02	8.39	5.52

Table 7.2. Maximum acceleration, velocity, displacement, and JMA seismic intensity (EW)

	Max Acc. [cm/s ²]	Max Vel. [cm/s]	Max Dis. [cm]	Seismic intensity
Main shock 15-80s	958.03	49.30	10.87	5.62
Bedrock wave	350.95	30.08	10.42	4.93
Z01	622.00	44.07	11.86	5.41
Z02	763.00	61.31	11.29	5.57
Z03	402.00	43.81	12.20	5.14
Z04	596.00	57.86	11.28	5.41

Table 7.3. Maximum acceleration, velocity, displacement, and JMA seismic intensity (vector sum)

	Max Acc. [cm/s ²]	Max Vel. [cm/s]	Max Dis. [cm]	Seismic intensity
Main shock 15-80s	1511.22	58.07	10.95	6.15
Bedrock wave	475.96	30.87	12.00	5.24
Z01	1008.81	50.58	12.08	5.85
Z02	1498.14	64.28	12.26	6.18
Z03	619.92	47.65	12.44	5.53
Z04	632.99	59.11	11.36	5.68

8. SUMMARY AND CONCLUSIONS

Temporary aftershock observation was undertaken near the K-NET Tsukidate in order to investigate the factors causing large acceleration near K-NET Tsukidate, as well as to understand the relationship of the large acceleration to building damages in the surrounding area. The amplification characteristics of the nearby soil structure were studied based on the H/V spectral ratio of the observed data.

A clear directional dependence was observed in the HVR at K-NET Tsukidate, which is indicative of the effect of topography. Small peaks at 0.3 Hz and 1.0 Hz were consistently observed near K-NET Tsukidate, which is attributed to the effect of the deep soil structure. While varying wave shapes were observed at each observation site above 1.5 Hz, waves of 7~10 Hz at MYG004 were the greatest among all observation sites. This corresponds to the amplification that can be seen in a linear microtremor array across the cliff for waves of frequencies above 7 Hz. Comparisons were made between the main shock on March 11th as well as the maximum aftershock on April 7th. Prolongation

of peak period was observed, which can be attributed to the effect of the nonlinearity of the soil structure.

The one-dimensional soil structure at K-NET Tsukidate was also identified based on the diffuse field theory. We were able to reproduce the peaks at 0.3 Hz and 1.0 Hz by increasing the depth of the layer with $V_s=3,400$ m/s to 2,900 m, resulting in the identification of a structure that matches the observed data very well. The soil structures at the temporary aftershock observation sites near Tsukidate were also identified. Although we were able to identify soil structures that match the observed data very well, there are differences in the deep soil structures and further identification is needed to obtain a homogeneous deep soil structure.

One-dimensional deconvolution analysis was applied to derive the incident seismic wave on the bedrock, which was found to have a maximum acceleration of 449 cm/s^2 in the NS direction and 350 cm/s^2 in the EW direction for the initial half of the whole duration. However, the actual soil structure is three-dimensional, and a detailed study would be needed to see two- and three-dimensional site effects. Based on strong-motion simulation using the deconvolved incident wave at the bedrock during the main shock at the temporary observation sites, it is estimated that despite a significant seismic intensity at the Tsukidate area due to large acceleration, the seismic motion did not cause structural damage to buildings because the main component of the motion was amplified only in the high-frequency range. The present strong-motion simulations only used the initial half of the recorded data from the main shock, and further simulations that consider the whole wave would be needed to perform in future.

AKCNOWLEDGEMENTS

We would like to thank all households of Tsukidate and the People of kawase-Matsushima laboratory in DPRI who cooperated in the measurement of aftershocks. We also thank the National Research Institute for Earth Science and Disaster Prevention (NIED) for allowing us to access to their K-NET data. Some of the figures were made using "Google Map". Partial support from DGAPA-UNAM under projects IN121709 and IN104712 is gratefully acknowledged.

REFERENCES

- Kawase, H. and Matsuo, H. (2004). Separation of Source, Path, and Site Effects based on the Observed Data by K-NET, KiK-net, and JMA Strong Motion Network. *Journal of JAE* **4:1**, 33-52 (in Japanese with English abstract).
- Kawase, H., Sanchez-Sesma, F. J. and Matushima, S. (2011). The Optimal Use of Horizontal-to-Vertical Spectral Ratios of Earthquake Motions for Velocity Inversions Based on Diffuse-field Theory for Plane Waves. *Bulletin of the Seismological Society of America* **101:5**, 2011-2014.
- Sanchez-Sesma, F. J., Rodriguez, M., Iturraran-Viveros, U., Luzon, F., Campillo, M., Margerin, L., Garcia-Jerez, A., Suarez, M., Santoyo, M. A. and Rodriguez-Castellanos, A. (2011). A theory for microtremor H/V spectral ratio: Application for a layered medium, *Geophys. J. Int.* **186:1**, 221-225..
- Kinoshita, S. (1998). Kyoshin Net (K-Net). *Seismological Research. Letters*, **69**, 309-334.
- National Research Institute for Earth Science and Disaster Prevention (2011). A strong-motion seismograph networks Portal site. http://www.kyoshin.bosai.go.jp/index_en.html .